THE JOURNAL OF BIOLOGICAL CHEMISTRY VOL. 289, NO. 37, pp. 25445–25459, September 12, 2014

An Essential Role for the K^+-dependent Na^+/Ca^{2+}-exchanger, NCKX4, in Melanocortin-4-receptor-dependent Satiety*

Received for publication, March 10, 2014, and in revised form, July 21, 2014 Published, JBC Papers in Press, August 5, 2014, DOI 10.1074/jbc.M114.564450

Xiao-Fang Li and Jonathan Lytton[1]

From the Department of Biochemistry and Molecular Biology, Hotchkiss Brain Institute and Libin Cardiovascular Institute of Alberta, Faculty of Medicine, University of Calgary, Calgary, Alberta T2N 4Z6, Canada

Background: The melanocortin-4 receptor, MC4R, regulates satiety, but the signaling mechanism is unknown.
Results: K^+-dependent Na^+/Ca^{2+}-exchanger, NCKX4, knock-out mice are lean and hypophagic and display MC4R-dependent, Ca^{2+}-sensitive, constitutive activation of paraventricular nucleus neurons.
Conclusion: Ca^{2+} signaling is required for MC4R action, and its dysregulation in *Nckx4*$^{-/-}$ mice leads to anorexia.
Significance: MC4R-mediated satiety requires NCKX4-modulated Ca^{2+} signaling.

K^+-dependent Na^+/Ca^{2+}-exchangers are broadly expressed in various tissues, and particularly enriched in neurons of the brain. The distinct physiological roles for the different members of this Ca^{2+} transporter family are, however, not well described. Here we show that gene-targeted mice lacking the K^+-dependent Na^+/Ca^{2+}-exchanger, NCKX4 (gene *slc24a4* or *Nckx4*), display a remarkable anorexia with severe hypophagia and weight loss. Feeding and satiety are coordinated centrally by melanocortin-4 receptors (MC4R) in neurons of the hypothalamic paraventricular nucleus (PVN). The hypophagic response of *Nckx4* knock-out mice is accompanied by hyperactivation of neurons in the PVN, evidenced by high levels of c-Fos expression. The activation of PVN neurons in both fasted *Nckx4* knock-out and glucose-injected wild-type animals is blocked by Ca^{2+} removal and MC4R antagonists. In cultured hypothalamic neurons, melanocyte stimulating hormone induces an MC4R-dependent and sustained Ca^{2+} signal, which requires phospholipase C activity and plasma membrane Ca^{2+} entry. The Ca^{2+} signal is enhanced in hypothalamic neurons from *Nckx4* knock-out animals, and is depressed in cells in which NCKX4 is overexpressed. Finally, MC4R-dependent oxytocin expression in the PVN, a key essential step in satiety, is prevented by blocking phospholipase C activation or Ca^{2+} entry. These findings highlight an essential, and to our knowledge previously unknown, role for Ca^{2+} signaling in the MC4R pathway that leads to satiety, and a novel non-redundant role for NCKX4-mediated Ca^{2+} extrusion in controlling MC4R signaling and feeding behavior. Together, these findings highlight a novel pathway that potentially could be exploited to develop much needed new therapeutics to tackle eating disorders and obesity.

Ca^{2+} homeostasis is a critical determinant of neuronal excitability via an influence on resting membrane potential, neurotransmitter release, and synaptic efficiency (1). Although ion channel activation is responsible for a rapid increase in Ca^{2+} levels, longer term regulation of Ca^{2+} depends mostly on extrusion pathways (2). Principal among these, particularly in neurons (3, 4), is the family of K^+-dependent Na^+/Ca^{2+}-exchangers (NCKX1 to -5),[2] encoded by the *slc24* genes (5, 6). NCKX family members are broadly expressed in various tissues, and particularly enriched in neurons of the brain. With the exception of NCKX1 (rod photoreceptors (7)) and NCKX5 (skin pigmentation (8)), the distinct physiological roles for the different family members are not well described. Recently published studies have shown an important role for NCKX4 (the product of the *slc4a4* or *Nckx4* gene) in olfactory function (9) and in tooth enamel formation (10). Our laboratory has independently generated *Nckx4*$^{-/-}$ mice, and we demonstrate here that adult animals display a remarkable hypothalamic defect that results in a dramatic anorexic and hypophagic phenotype.

The hormonally regulated and neuronally encoded network that controls food intake, satiety, and energy homeostasis is the major determinant of body weight in both animal models and humans (11–13). Peripherally produced circulating factors, such as insulin and leptin, influence energy balance through their action on neuronal centers within the hypothalamus, primarily in the arcuate nucleus (ARC) (12). Here, two classes of neurons have antagonistic effects on feeding behavior. One class express neuropeptide Y and agouti-related protein (AgRP) and induce feeding, whereas the other class express pro-opiomelanocortin (POMC; the precursor to melanocortins, such as α-melanocyte stimulating hormone (MSH), adrenocorticotropic hormone and the endorphins) and suppress feeding (14). Leptin acts to inhibit AgRP neurons whereas stimulating

* This work was supported in part by Canadian Institutes of Health Research Grant FRN 97876 (to J. L.).
[1] Supported by a Tier 1 Canada Research Chair and an Alberta Innovates-Health Solutions Medical Scientist award. To whom correspondence should be addressed: University of Calgary, Health Research Innovation Centre, Rm. GAC64, 3280 Hospital Dr. NW, Calgary, AB T2N 4Z6, Canada. Tel.: 403-220-2893; Fax: 403-210-8105; E-mail: jlytton@ucalgary.ca.

[2] The abbreviations used are: NCKX, K^+-dependent Na^+/Ca^{2+}-exchanger; ARC, arcuate nucleus of the hypothalamus; AgRP, *Agouti*-related peptide; MC4R, melanocortin-4 receptor; MSH, α-melanocyte stimulating hormone; OXT, oxytocin; PLC, phospholipase C; POMC, pro-opiomelanocortin; PVN, paraventricular nucleus of the hypothalamus; TRPC, transient receptor potential channel.

POMC neurons. The targets of POMC and AgRP neurons are principally melanocortin-4 receptor (MC4R) expressing neurons found in the paraventricular nucleus (PVN) as well as other hypothalamic areas (11–13). MSH, released from POMC neurons, is an agonist for MC4R and acts to stimulate the firing rates of downstream neurons (15). AgRP, on the other hand, is an antagonist of MC4R, thereby inhibiting these neurons (11–13, 15), although AgRP neurons have also been shown to induce feeding directly, without melanocortin involvement (14, 16).

Loss of function of the MC4R in mouse models causes profound obesity, due to both hyperphagia and reduced energy expenditure (17). Targeted knock-out and re-expression of MC4R in the PVN has established this as the key hypothalamic site for the regulation of feeding behavior (18, 19). Importantly, mutations in MC4R are the most abundant monogenetic cause of obesity in humans, and a relatively common cause of severe obesity in childhood (20). Moreover, there is emerging evidence that MC4R variants contribute to obesity more generally (21). These observations have focused attention on the central melanocortin system as the essential control network for the regulation of energy homeostasis (11), with MC4R-expressing neurons as the core element (22). The MC4R is a G-protein coupled receptor that can stimulate $G\alpha_s$ and consequently activate adenylyl cyclase to increase cAMP levels (22). However, a causative role for cAMP in MC4R signaling that leads to satiety has not to our knowledge been demonstrated. Indeed, loss of $G\alpha_s$ function in PVN does not influence feeding behavior (23, 24). Thus, the mechanism that links MC4R signaling to changes in neuronal firing, and particularly to the control of feeding behavior, remains unknown.

We demonstrate here that genetically targeted *Nckx4*$^{-/-}$ mice lacking the NCXK4 protein display a striking anorexic phenotype as a consequence of Ca^{2+}-dependent heightened sensitivity of MC4R in the PVN. These data also demonstrate an essential role for Ca^{2+} signaling downstream from MC4R in mediating feeding behavior and satiety.

EXPERIMENTAL PROCEDURES

Animals—Mice were maintained and treated in accordance with the guidelines of the Canadian Council on Animal Care as determined by the University of Calgary Animal Care Committee. *Mc4r* knock-out mice (loxTB *Mc4r* mice (19)) were purchased as heterozygous animals from Jackson Laboratory (stock number 006414). C57Bl/6 mice used for breeding with chimeric animals were obtained from Charles River. All mice were kept in a pathogen-free environment with a 12-h light/dark schedule, and were maintained *ad libitum* on a commercial diet (20% protein, 9% fat, and 4% fiber; PMI Nutrition International LLC, catalog number 5062), with free access to water.

Generation of Nckx4$^{-/-}$ *Knock-out Mice*—A conventional gene targeting approach was taken to produce a constitutive knock-out of the mouse *slc24a4* (*Nckx4*) gene by deletion of exons 6 and 7, as illustrated in Fig. 1. Briefly, *Nckx4* fragments were amplified from mouse 129/SvJ genomic DNA by PCR using a high-fidelity polymerase, and combined in pBluescript II SK(−) (Agilent Technologies) with a polymerase II promoter-driven neomycin resistance cassette (25), and the herpes simplex virus promoter-driven thymidine kinase gene derived from the pflox vector (26) (see Fig. 1). A linear NotI fragment of 11.7 kb was isolated, electroporated into E14 embryonic stem cells derived from the 129P2/Ola mouse line, and recombinants were screened using positive/negative selection as previously described (25). Targeted cells were then screened by Southern blot as described below to confirm homologous recombination. Blastocyst injections led to two male chimeras that were then bred with C57Bl/6 females, and agouti animals were screened by Southern blot to identify recombinant *Nckx4* heterozygous animals. Subsequent animal genotyping was conducted using a mixed PCR primer protocol (see below). Both chimeric mice resulted in targeted *Nckx4* heterozygotes, creating two independent lines. Most studies were performed on F2/F3 animals from one line, using littermates of different genotypes for comparison. The anorexia and hypophagia reported here was confirmed in animals from the second line (data not shown). Embryonic stem cell targeting and chimeric mouse production were conducted at the Clara Christie Center for Mouse Genomics, Faculty of Medicine, University of Calgary.

Mc4r$^{+/-}$ heterozygous male mice were bred with *Nckx4*$^{+/-}$ heterozygous females to produce animals that were doubly heterozygous for both genes. Then the double heterozygotes were bred together sequentially to produce the double knock-out. Mice at 3–4 months of age were used for food intake experiments and c-Fos staining, body weight was measured in 5–6-month-old animals.

Chemicals—All chemicals used were analytical or molecular biology grade or better, and generally obtained from Sigma or VWR International, unless indicated otherwise.

Construction of Lentivirus Containing Mouse Nckx4—The *Nckx4* cDNA in pcDNA3.1+ (Invitrogen) has been previously described (27). A fragment from the pWPI vector (a kind gift of Dr. Didier Trono obtained as Addgene plasmid 12254) encompassing the central polypurine tract (cPPT), internal ribosome entry site (IRES), and enhanced green fluorescent protein (EGFP) loci was inserted at the 3′ end of the *Nckx4* cDNA. A fragment comprising the CaMKIIa promoter from the pLenti-CamKII-ChETA-EYFP (a kind gift of Dr. Karl Deisseroth obtained as Addgene plasmid 26967) (28) was inserted at the 5′ end of the *Nckx4* cDNA. The entire CaMKIIa-promoter-Nckx4-IRES-EGFP construct was then excised as an XbaI-EcoRI fragment and used to replace the corresponding CaMKIIa-promoter-ChETA-EYFP fragment from the pLenti vector. This construct was propagated in Stbl3 *Escherichia coli* cells (Invitrogen). A control construct was also generated in which most of the NCKX4 coding region was removed by BamHI digestion and ligation. These constructs were then packaged and amplified by transfection into HEK293T cells using the helper plasmids pMD2.G and psPAX2 (both kind gifts of Dr. Didier Trono obtained as Addgene plasmids 12259 and 12260) as described on the Trono laboratory website. Final viral particles were concentrated by centrifugation and collected on a 20% sucrose cushion in PBS.

Molecular Analyses—All molecular biology procedures were conducted essentially according to standard protocols (29). Genomic DNA was isolated by phenol/chloroform extraction from adult mouse liver, targeted ES cells, or mouse tail snips for genotyping. For Southern blot analysis, ~10 μg of genomic

DNA was digested overnight with NsiI, separated on a 1% agarose gel, transferred to nylon, and probed with a digoxigenin-labeled genomic fragment located upstream of the targeting *Nckx4* sequence. This probe recognizes a 9.9-kb band in genomic DNA from wild-type animals, and a 4.9-kb band in the targeted allele (see Fig. 1). For mixed PCR genotyping, we employed a forward primer (P1: CCATACTAACGATGATGATGGTG) immediately upstream of exon 6, a reverse primer (P2: GAACACAGCAGAGCCCACAAT) located within exon 6, and a reverse primer (P3: CGGGCCTCGTTCATGAATATTC) from the murine polymerase II promoter at the 5′-end of the neomycin resistance cassette. Amplification from wild-type genomic DNA resulted in a band of 175 bp between primers P1 and P2, whereas amplification from the targeted locus resulted in a band of 350 bp between primers P1 and P3. The PCR genotyping analysis of the loxTB *Mc4r* mice was performed in a similar manner, essentially according to the published report (19).

Total RNA was isolated by guanidinium isothiocyanate extraction and CsCl centrifugation. For Northern blot analysis, 10 μg of total RNA was separated by formaldehyde-agarose gel electrophoresis, transferred to nylon, and analyzed at high stringency essentially as described previously (30) using a digoxigenin-labeled probe corresponding to exon 6 and exon 7 of mouse *Nckx4*. The probes and conditions for detection of *Ncx1*, *Ncx2*, *Ncx3*, *Nckx2*, and *Nckx3* transcripts were as described previously (30).

For immunoblot analysis, a membrane fraction, enriched in synaptic markers, was isolated from homogenized whole brains of mice of each genotype according to published procedures (30). Aliquots of 25 μg of this membrane fraction were separated by SDS-PAGE, transferred to nitrocellulose membranes, and probed with an antibody against NCKX4. The NCKX4 antibody was prepared by immunizing rabbits with a keyhole limpet hemocyanin-conjugated peptide (CVKEKPPYGKTPVVMV) from the cytoplasmic loop of the mouse NCKX4 protein (amino acids 294–308; N-terminal Cys residue added for conjugation) in the University of Calgary Faculty of Medicine Antibody Services Facility. Anti-NCKX4 antibody was affinity purified from serum with immobilized peptide using the SulfoLink kit (Pierce-Thermo Scientific).

In situ hybridization was performed with digoxigenin-labeled antisense/sense riboprobes corresponding to nucleotides 680–1398 of mouse *Nckx4* essentially as described previously (30) on 7-μm coronal paraffin sections cut sequentially across the entire hypothalamic region of mouse brain.

Behavioral Screen—Ten age-matched mice of each genotype and sex at 4–5 months of age were characterized using established methods (31). Measures of general health and behavior were determined: general appearance, body weight, whisker length and appearance, and fur appearance. Nest building, social huddling, and general behaviors including social interactions and fighting were monitored in the home cage for any aberrant activity. Evidence of tremors, twitches, or seizures was recorded. The following neurological and sensory reflexes were observed for individual animals: righting reflex, postural reflex, eye blink reflex, ear twitch reflex, whisker orienting reflex, forelimb placing reflex, hind limb placing reflex, acoustic startle reflex, tail flick response, and visual placing test. The animals were also subject to an open field test and measures of distance traveled, time spent resting, and time spent in ambulatory activity recorded (Auto-Track system; Columbus Instruments). No abnormalities were observed in any of the general health and behavioral parameters, nor were there statistically significant differences in the open field measures. A wire-hang test was also performed, but the difference in mass between genotypes confounded the analysis of these data, which are not reported.

Weight Gain Curves—A subset of mice were weighed immediately after birth (P0) and a tail snip taken for genotyping. All other mice were routinely weighed upon weaning when they were separated into cages by sex, identified by ear punch and genotyped. Subsequently, these mice were weighed individually once a week in the morning of the same day, from weaning up to 32 weeks of age. Separate sets of animals were allowed free access to either the normal "enriched" lab chow containing 9% fat by weight (PMI Nutrition International LLC, catalogue 5062), "low fat" regular lab chow (4.5% fat by weight; Harlan Teklad, catalogue 5002), or a high fat diet (22.8% fat by weight; Harlan Teklad, catalogue TD.06415). Diets were introduced at the time of mating of the heterozygous parents of the animals used in the studies. The data were classified according to gender and genotype to construct weight gain curves. Not all animals of all genotypes on all diets were measured at all time periods. Data are thus only reported up to 24 weeks of age. The high fat diet tended to be rejected such that animals fed this diet did not weigh more than those on the enriched 9% fat lab chow. These data are therefore not reported.

Animal Morphology—A select set of adult mice (5–6 months old) were sacrificed by injection with a lethal dose of sodium pentobarbital. The animals were then weighed, and their length determined from nose to anus by gently straightening the spine. Heart, kidneys, liver, and total abdominal cavity fat mass (bilateral epididymal, inguinal, and retroperitonal fat pads) were dissected from these animals, blotted dry, and weighed. For tissue histology, mice were perfused transcardially with heparin (0.8 USP/ml) in 0.1 M phosphate buffer, pH 7.5, for 30 min, followed by 4% paraformaldehyde in 0.1 M phosphate buffer. Tissue was removed, fixed overnight in the same solution, paraffin embedded, and 7-μm sections were stained with hematoxylin and eosin. Tissue histology was performed in the Department of Pathology and Laboratory Medicine core laboratory at the University of Calgary.

Food and Water Intake—Food intake was measured on 5–6-month-old mice, each housed two or three to a cage, and allowed to habituate for at least a week before any measurements were taken. Over a 2-week period, a sufficient amount of food for the period was weighed and provided to the mice. Each weekday morning, the remaining food was measured, for a total of 10 measurements. Cages were carefully monitored for spillage, which was negligible. For water consumption, a measuring tube was constructed by inserting a normal mouse drinking tube with a rubber stopper into a 50-ml Falcon tube bearing volume marks. Daily water intake was measured for mice housed two to a cage each weekday morning over 2 weeks, for a total of 10 measurements. Special attention was given to limit

cage movement, to prevent water draining and spilling. The 10 measurements of food or water intake were averaged and normalized per mouse to generate an individual datum point per animal.

Hidden Item Olfaction Tests, Urine-scented Litter—This test was performed on 5–6-month-old mice, using a protocol adapted from published methods (32). A small amount of urine-scented litter from an animal of the opposite sex was hidden near one end of a clean cage (43 × 25 × 20 cm) filled with fresh litter to a depth of about 3 cm. An individual free-fed mouse was released at the other end of the cage, and the time taken before the mouse located and dug up the urine-scented litter was noted.

Buried Food Pellet—This test was performed on 7–9-month-old mice according to a previously published protocol (32). For three consecutive days before the experiment, a piece of Oreo cookie (Nabisco) was put into each cage, and checked next morning for consumption. Each tested mouse was then fasted for 24 h, and transferred into a clean cage containing fresh bedding for 5 min to allow the subject to acclimate to the cage. One piece of cookie (80–90 mg) was buried ~1 cm beneath the surface, in a corner of a clean testing cage containing fresh bedding as above. Then an individual mouse was transferred to the far end of the test cage, and the time taken to find and start to eat the cookie piece was recorded.

Blood Hormone and Chemistry Measurements—Blood samples were collected from 4–5-month-old overnight-fasted mice via cardiac puncture, clotted at room temperature for 30 min, and then spun down at 3000 × *g* for 15 min. The serum samples were supplemented with 1/10 volume of proteinase inhibitor mixture plus final concentrations of 200 μM PMSF and 0.3 μM aprotinin, divided into aliquots, and stored at −80 °C. Serum levels for glucose, triglyceride, cortisol, MSH, insulin, leptin, and total thyroxine were measured according to the manufacturer's instructions using kits from Sigma for glucose and triglyceride, ALPCO Diagnostics for cortisol and MSH, Linco Research for insulin and leptin, and MP Biomedicals for total thyroxine.

Glucose Tolerance Test—5–6-Month-old mice were fasted overnight and then injected with glucose solution (2 mg glucose/g body weight) into the peritoneal cavity. Glucose levels were measured in blood collected from the tail immediately before and 15, 30, 60, and 120 min after the injection using OneTouch blood glucose strips (OneTouch FastTake, Life Scan).

Body Temperature Measurements—Body temperature in 5–6-month-old mice was measured at ~9–10 a.m. each morning rectally using a BAT-12 microprobe thermometer from Physitemp Instruments.

Immunofluorescent Staining—Mice were anesthetized with pentobarbital and perfused transcardially with heparin (0.8 USP/ml) in 0.1 M sodium phosphate, pH 7.5, for 30 min, followed with 4% paraformaldehyde in 0.1 M sodium phosphate buffer, and the brains were removed and fixed overnight in the same solution. For antibody staining following *in vitro* perfusion conditions (treatments with insulin, MSH (Calbiochem, catalog number 05-23-075), SHU9119 (Bachem, catalog number H-3952), SKF96365 (Sigma), U73122 (EMD-Millipore), and Ca^{2+}-free Krebs-Henseleit plus 0.5 mM EGTA), mice were perfused transcardially for 30 min with heparin (0.8 USP/ml) in Krebs-Henseleit solution (124 mM NaCl, 3 mM KCl, 26 mM $NaHCO_3$, 2 mM $CaCl_2$, 2 mM $MgCl_2$, 1.25 mM NaH_2PO_4, 10 mM glucose, gassed with 95% O_2, 5% CO_2). Following treatment, animals were fixed by perfusion with 4% paraformaldehyde in 0.1 M sodium phosphate buffer, and the brains were removed and fixed overnight in the same solution. Immunofluorescent staining was performed on 50-μm free-floating brain coronal sections encompassing the entire hypothalamus area cut by vibratome. The sections were blocked for 2 h in working solution (3% donkey serum, 2% dimethyl sulfoxide, and 0.2% Tween 20 in 0.1 M sodium phosphate), incubated overnight at 4 °C with primary antibodies (against MSH (Bachem, catalog number T-4434) used at a dilution of 1:4000; AgRP (Phoenix Pharmaceuticals, catalog number H-003-57) used at a dilution of 1:500; c-Fos (Calbiochem, catalog number PC38 (Ab-5)) used at a dilution of 1:5000; oxytocin (EMD-Millipore, catalog number MAB5296) used at a dilution of 1:600) in working solution. After washing, the sections were incubated overnight at 4 °C with 1:500 dilutions in working solution of the appropriate Cy3 (Jackson ImmunoResearch Laboratories) species-related secondary antibody. After final washing, the sections were mounted in Vectashield anti-fade medium (Vector Labs) and viewed on a Zeiss Axioskop 2 microscope and fluorescent images were captured with a Spot RT3 camera system (Diagnostic Instruments).

Cell Culture, Ca^{2+} Imaging, and cAMP Determination—All cell culture solutions and reagents were obtained from Invitrogen. Immortalized murine hypothalamic GT1–7 cells (33) (a kind gift from Dr. Richard Weiner, University of California at San Francisco) were cultured in DMEM supplemented with 10% fetal bovine serum. Cells in either multiwall dishes or on poly-D-lysine-coated coverslips were grown to confluence and then used for all assays.

For lentiviral infection, GT1–7 cells at ~70–80% confluence were washed with Opti-MEM, then treated with lentivirus (multiplicity of infection of about 1) and Polybrene (8 μg/ml) in Opti-MEM for 6 h. Three volumes of regular culture medium was added to the virus-treated wells overnight, and this mixture was replaced with fresh culture medium the next morning. The cells were incubated a further 2 days before being used for all assays.

Primary hypothalamic neuronal cell cultures were obtained by dissecting the hypothalamus from E18–19 fetal or P0 neonatal mouse brain in ice-cold Hank's balanced salt solution (using the anterior margin of the optic chiasm, the posterior margin of the mammillary bodies, and the lateral hypothalamic fissures as guides), then digested with papain (Worthington Biochemicals) at 61.3 units/ml in basal medium Eagle (BME) containing 10% fetal bovine serum, and triturated with a fine glass pipette. The dissociated cells were pooled from the brains of 6 pups from each pregnant female, evenly plated on poly-D-lysine- and laminin-coated coverslips in 24-well plates and cultured in Neurobasal medium supplemented with 2% B27. The cultured neurons reached full confluence at 12–15 days, and were used for Ca^{2+} imaging and cAMP assays at this point.

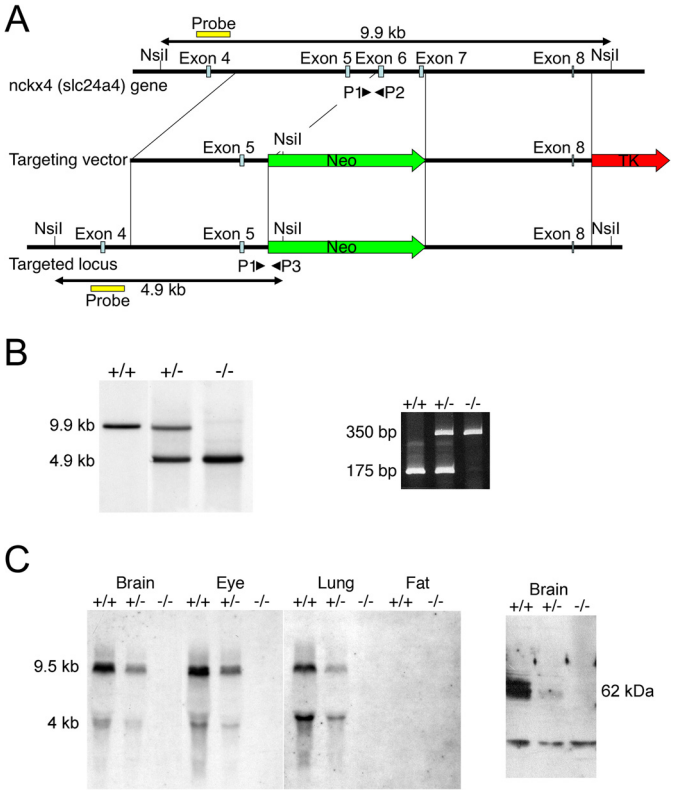

FIGURE 1. **Generation of *Nckx4*$^{-/-}$ knock-out mice.** *A,* diagram illustrating the *Nckx4* (*slc24a4*) locus, the targeting vector, and the targeted locus. The location of *Nckx4* exons 5, 6, 7, and 8 is indicated. The neomycin (*neo*) gene driven by a pol II promoter replaced exons 6 and 7 in the targeted locus. The thymidine kinase gene driven by a herpes simplex virus promoter was used for negative selection. The location of the probe used for Southern analysis and the length of the two diagnostic NsiI fragments of 9.9 and 4.9 kb are illustrated at the *top* and *bottom* of the diagram. The position of the primers used for PCR analysis, *P1*, *P2*, and *P3*, which generate diagnostic fragments of 175 or 350 bp are also indicated. *B,* genotype analysis by Southern blot (*left*) or PCR (*right*) of DNA from wild-type (+/+), heterozygous (+/−), or *Nckx4* knock-out (−/−) animals. *C,* Northern blot (*left panel*) analysis of 10 μg of total RNA samples, or immunoblot (*right panel*) analysis of 20 μg of membrane proteins samples, isolated from the indicated tissues of mice of different genotype.

For Ca^{2+} imaging, the cells were loaded with 5 μM fura-2 AM (Molecular Probes) for 45 min at room temperature, mounted in a Warner Instruments chamber on a Zeiss Axioskop FS2 microscope, and perfused with physiological solution containing 135 mM NaCl, 5 mM KCl, 2 mM $MgCl_2$, 2 mM $CaCl_2$, 10 mM Hepes, pH 7.5, and 30 mM glucose. Fura-2 ratio images were acquired at 10-s intervals at room temperature using the EasyRatioPro system from Photon Technology International. Data were analyzed by placing regions of interest around responding cells.

For the cAMP assay, cultured cells were washed and incubated with Opti-MEM containing 0.5 mM isobutylmethylxanthine for 10 min, then stimulated with various concentrations of MSH for 15 min at 37 °C. The medium was aspirated, and the cells were lysed in 0.1 M HCl. cAMP levels were measured following the manufacturer's instructions using ELISA kits from Biovision Research Products.

Statistics—Data were analyzed by either *t* test (in the case of only two test groups) or analysis of variance followed with the Bonferroni post-test to determine statistical significance, calculated using either GraphPad Prism or Microsoft Excel.

RESULTS

Nckx4$^{-/-}$ *Mice Are Anorexic and Hypophagic*—The expression of NCKX4 was disrupted constitutively using a conventional gene targeting approach directed to the *slc24a4 (Nckx4)* gene (see Fig. 1). This was confirmed at the transcript level in brain, eye, and lung (tissues that normally express higher levels of *Nckx4* (34)) using a probe from the deleted exons, and at the protein level in brain using an anti-peptide antibody. These data demonstrate complete absence of the NCKX4 protein in targeted *Nckx4*$^{-/-}$ animals (Fig. 1*C*). The *Nckx4* gene is broadly expressed in brain (see Fig. 2*A*), but there was no obvious difference in brain morphology in the knock-out animals (see Fig. 2*B*), nor any compensatory change in expression of paralogous Na^+/Ca^{2+}-exchanger genes in *Nckx4*$^{-/-}$ mice (Fig. 2*C*). The knock-out mice were viable, overtly healthy and fertile, and heterozygous breeding resulted in the expected Mendelian ratio of *Nckx4* inheritance. A basic standard behavioral screen (31) displayed no abnormalities in the knock-out animals.

In contrast to the otherwise normal phenotype of the mice, an obvious reduction in body mass of the *Nckx4*$^{-/-}$ animals was immediately evident (Fig. 3). Although not present at birth (Fig. 3*B*), the difference was already significant at weaning (4 weeks of age; Fig. 3*B*), and reached a sustained reduction of about 25–30% at 4 months of age (Fig. 3*C*). A similar fractional reduction in body mass was observed when knock-out animals were fed either standard lab chow (4.5% fat) or an enriched diet (9% fat) (Fig. 3*A*). Heterozygous *Nckx4* animals were not different in weight from wild-type. In contrast to the reduction in the weight of knock-out animals, there was no change in their body length (Fig. 3*C*). The reduction in body weight was accompanied by a proportional reduction in food consumption, and a modest but statistically significant reduction in water intake (Fig. 3*D*). The knock-out mice also displayed reduced abdominal fat tissue with smaller adipocytes, and smaller, less fatty, livers (Fig. 4). The *Nckx4*$^{-/-}$ animals did not display elevated body temperature (Fig. 4*A*) nor higher than normal T4 levels (Fig. 6*A*), and thus the reduced body mass appears to be almost entirely a result of the hypophagic phenotype.

The Hypophagia of Nckx4$^{-/-}$ *Mice Is Not Secondary to Other Health Issues*—The knock-out mice do not display any pervasive development defect, as indicated by their normal birth weight, normal length, and normal brain morphology (see Figs. 2 and 3). In addition, the knock-out animals display improved glucose utilization, and a modestly extended lifespan (Fig. 5, *A* and *B*), consistent with previous studies on animals fed calorie-restricted diets (35). Moreover, motivational problems do not seem to underlie the hypophagia. First, *Nckx4* knock-out mice demonstrated a paradoxical small increase in food consumed immediately following a 24-h fast (Fig. 5*C*). Similar behavior has been observed in other genetically lean mice (36), and has been attributed to depleted energy reserves in fasted animals. Second, the knock-out mice performed slightly better than controls in the task of finding hidden urine-scented litter (Fig. 5*D*). On the other hand, the *Nckx4*$^{-/-}$ mice took longer to find a buried food pellet (Fig. 5*D*).

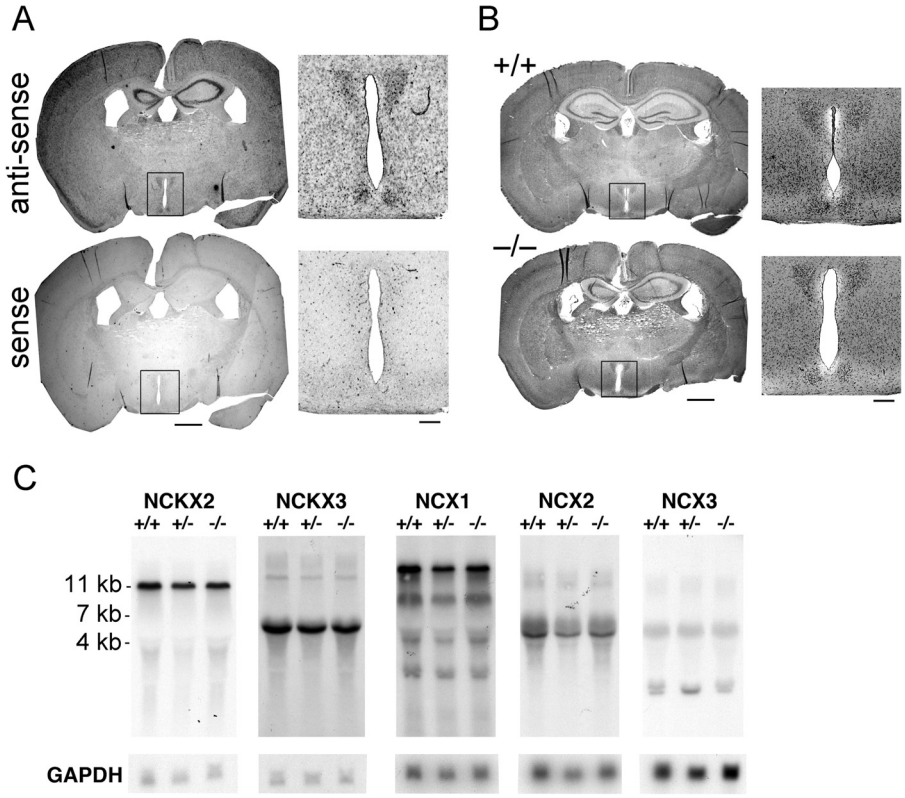

FIGURE 2. ***Nckx4* knock-out does not change brain morphology or the expression of other Na^+/Ca^{2+}-exchangers.** *A,* serial coronal sections through the hypothalamus of wild-type adult mice were labeled for *Nckx4* transcripts with an antisense or a sense control probe, as indicated. *B,* hematoxylin and eosin-stained coronal paraffin sections through the PVN (wild-type, +/+; *Nckx4* knock-out, −/−). No differences were observed between genotypes in this or in other brain regions examined in either coronal or parasagittal stained sections (data not shown). In both *panels A* and *B*, the *right-hand* images are magnified views of the area in the *box* in the corresponding *left-hand* images. *Scale bars*: left-hand images, 1 mm; right-hand images, 200 μm. *C,* Northern blots of 10 μg of total RNA samples isolated from adult brain of wild-type (+/+), heterozygous (+/−), or *Nckx4* knock-out (−/−) mice were analyzed with probes for the indicated Na^+/Ca^{2+}-exchangers genes. The blots were then stripped and reprobed for *Gapdh* as a loading control. All images in this figure are representative of independent experiments from 3 different animals of each genotype.

MC4R-dependent and Ca^{2+}-sensitive Hyperactivation of PVN Neurons Underlies the $Nckx4^{-/-}$ Phenotype—Chronic elevation of peripheral adiposity factors would lead to hypophagia (11–13). However, insulin, leptin, glucose, and MSH were all significantly lower in the $Nckx4^{-/-}$ mice than in wild-type controls (Fig. 6*A*). The direction of these changes is indicative of a fasted, or semi-starved, state that would normally increase feeding, rather than reduce it.

In the hypothalamic ARC, satiety and feeding cessation are signaled from POMC neurons by an increase in the synthesis and release of anorexigenic MSH, and by inhibition of the synthesis and release of orexigenic AgRP and neuropeptide Y from their cognate neurons (11–13). Immunofluorescent analysis of brain sections illustrates the typical punctate pattern of packaged peptide hormone expression (Fig. 6*B*). However, the knock-out animals displayed paradoxically decreased MSH and increased AgRP levels in the ARC compared with wild-type, which therefore rules out these mediators as the cause for hypophagia.

The PVN is one of the major sites of neuronal activation upon feeding (37), and a selective role in food intake has been demonstrated here for the MC4R (11, 18, 19). Therefore, we examined neuronal activation in PVN under different physiological states in both wild-type and *Nckx4* mutant mice, using c-Fos expression as a marker. As seen in Fig. 7, glucose infusion into fasted wild-type mice induced an obvious and highly significant 4-fold increase in the number of c-Fos positive cells, which was blocked by treatment with the MC4R antagonist, SHU9119. Infusion of insulin to previously fasted mice also induced a similar increase in c-Fos expression in the PVN, suggesting the effect of glucose may be in part secondary to insulin release. In contrast, fasted *Nckx4* knock-out mice displayed a density of c-Fos staining in the PVN that was equivalent to the numbers observed in the glucose- or insulin-treated wild-type controls (Fig. 7). Moreover, the constitutive activation of PVN neurons in the knock-out was blocked by SHU9119 treatment, even though MSH release is expected to be suppressed under these conditions. This observation suggests that the MC4R in PVN is constitutively activated, or hyper-sensitized, in *Nckx4* knock-out mice. Ca^{2+} chelation with EGTA also reduced the level of c-Fos expression observed in the knock-out, indicating a role for altered Ca^{2+} homeostasis due to loss of the NCKX4 protein. These data indicate that constitutive hyperactivation of PVN neurons, which is both MC4R-dependent and Ca^{2+}-sensitive, plays a key role in the hypophagic phenotype of $Nckx4^{-/-}$ mice.

To test further the role for MC4R in the *Nckx4* knock-out phenotype, $Nckx4^{-/-}$ and $Mc4r^{-/-}$ (19) mice were bred together to create a double knock-out. While $Nckx4^{-/-}$ mice displayed decreased food consumption and body weight, and

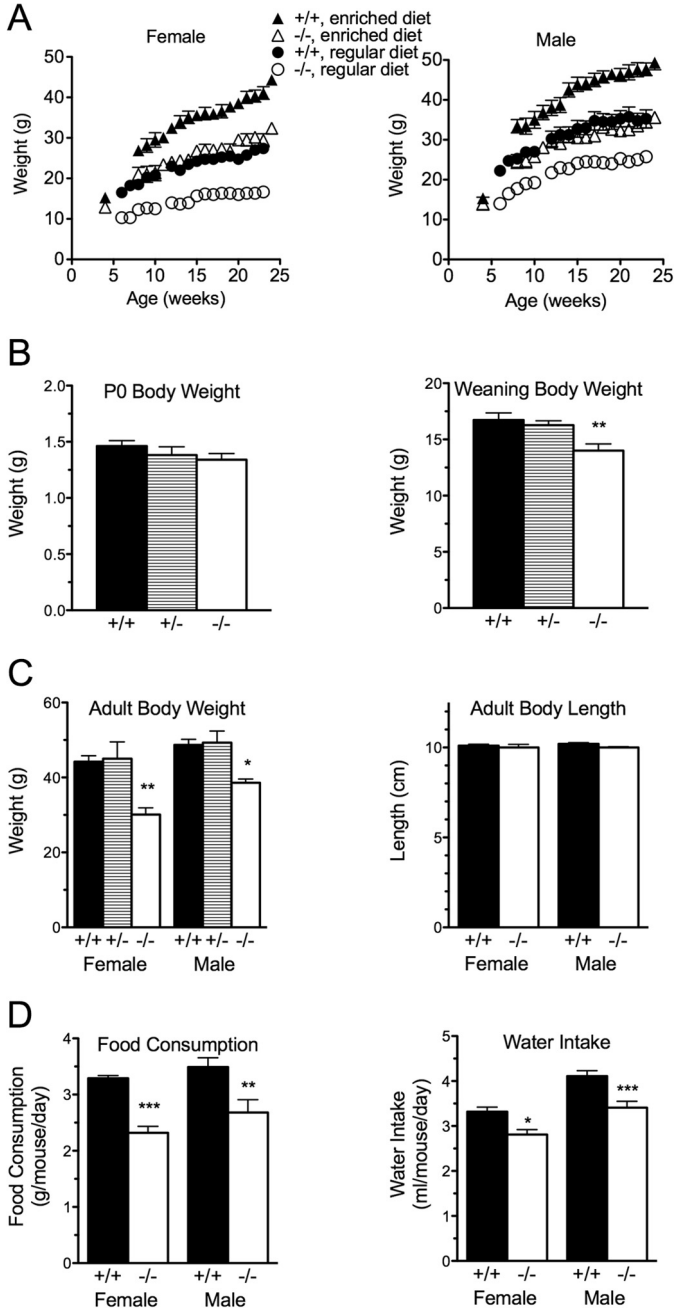

FIGURE 3. ***Nckx4*$^{-/-}$ mice are anorexic and hypophagic.** Knock-out (−/−) and wild-type (+/+) and heterozygous (+/−) littermates, as indicated, were fed *ad libitum* either standard or enriched laboratory chow (4.5% or 9% fat). *A,* animals were weighed weekly from 4 weeks of age onwards ($n = 12–15$ for each group; however, measurements were not made for all animals for all time points, all conditions or both sexes; therefore, some data points correspond to a smaller *n* value). *B*, animals were weighed at birth (P0; $n = 10$) and then at weaning ($n = 63$, 107, and 56 for wild-type, heterozygous, and knock-out, respectively). *C,* weight ($n = 8$) and length (nose to anus; $n = 10$) were measured on adult animals. *D,* food ($n = 8$ for females and $n = 10$ for males) and water consumption ($n = 6$) were measured in adult animals. In all cases the mean ± S.E. is plotted. Statistical significance of differences between knock-out and wild-type is indicated where present: *, $p < 0.05$; **, $p < 0.01$; ***, $p < 0.001$.

increased c-Fos expression in the PVN, *Mc4r*$^{-/-}$ mice displayed the opposite responses: increased food consumption and body weight, and decreased c-Fos expression in PVN (Fig. 8). The double knock-outs were indistinguishable in response to the *Mc4r*$^{-/-}$ mice and significantly different from either *Nckx4*$^{-/-}$ mice or wild-type controls (Fig. 8). These data support an essential role for MC4R signaling in the etiology of the *Nckx4* knock-out phenotype.

MC4R-induced Ca^{2+} Signals in Hypothalamic Neurons—The loss of exchanger-driven Ca^{2+} extrusion would be anticipated to influence Ca^{2+} homeostasis and signaling. Therefore, Ca^{2+} signaling was examined in cultured hypothalamic neurons from wild-type and *Nckx4* knock-out mice. Treatment with MSH induced a Ca^{2+} response in a minority of hypothalamic neurons, consistent with the fraction of cells expected to express MC4R (19). The character of the response was highly variable from cell to cell within one microscopic field, with individual cells displaying either a single transient spike; repetitive, prolonged, oscillatory behavior; or delayed but sustained Ca^{2+} elevation (Fig. 9*A*). Extensive time control experiments confirmed that these Ca^{2+} signals were dependent upon treatment with MSH. The *Nckx4*$^{-/-}$-derived cultures consistently displayed a larger number of cells responding to MSH stimulation per field (Fig. 9*B*). Otherwise, there were no obvious alterations in the magnitude or time course of Ca^{2+} signals in the knock-out cells, including their response to KCl treatment. Collectively, these data indicate that loss of NCKX4 leads to a highly selective MSH hyper-responsive state that involves altered Ca^{2+} signaling, and which can account for the constitutive activation of PVN neurons and downstream satiety pathways in the *Nckx4*$^{-/-}$ animals.

MC4R-positive neurons represent only a minor component of all hypothalamic neurons, and so to study further the Ca^{2+} response to receptor stimulation, we utilized an immortalized murine hypothalamic cell line, GT1–7 (33), known to express MC4R (38), but which has lost NCKX4 expression. GT1–7 cells were infected with lentivirus expressing mouse NCKX4 or a control construct, and Ca^{2+} signals were recorded in response to MSH stimulation. As seen in Fig. 9*C*, these signals were very similar, in their variable and oscillatory temporal behavior, to those observed in the cultured hypothalamic neurons. Expression of NCKX4 in GT1–7 cells caused a significant reduction in the number of responding cells (Fig. 9*D*), analogous to the observations in hypothalamic neurons from wild-type *versus* knock-out mice.

The Ca^{2+} signals in response to MSH treatment were examined in more detail, as shown in Fig. 10. The response typically continued long after wash-out of MSH (Fig. 10, *A*, *D*, *G*, and *H*), and was completely blocked by the MC4R antagonist, SHU9119 (Fig. 10*B*). The induced Ca^{2+} signals required the presence of extracellular Ca^{2+}, such that its removal both abolished previously activated signals and prevented the development of signals when removed prior to the MSH stimulus (Fig. 10, *C* and *D*). Importantly, there was no evidence for transient Ca^{2+} release from ER stores in response to MSH in the absence of extracellular Ca^{2+} (Fig. 10*D*). Subsequent re-addition of Ca^{2+} after MSH had been washed out led to resumption of the typical oscillatory Ca^{2+} response (Fig. 10*D*). The MSH-induced Ca^{2+} response was also prevented by prior treatment with the phospholipase C (PLC) inhibitor, U73122, or with the TRPC-selective Ca^{2+}-entry inhibitor, SKF96365, but not with the voltage-dependent Ca^{2+} channel inhibitor, nifedipine, or the cAMP

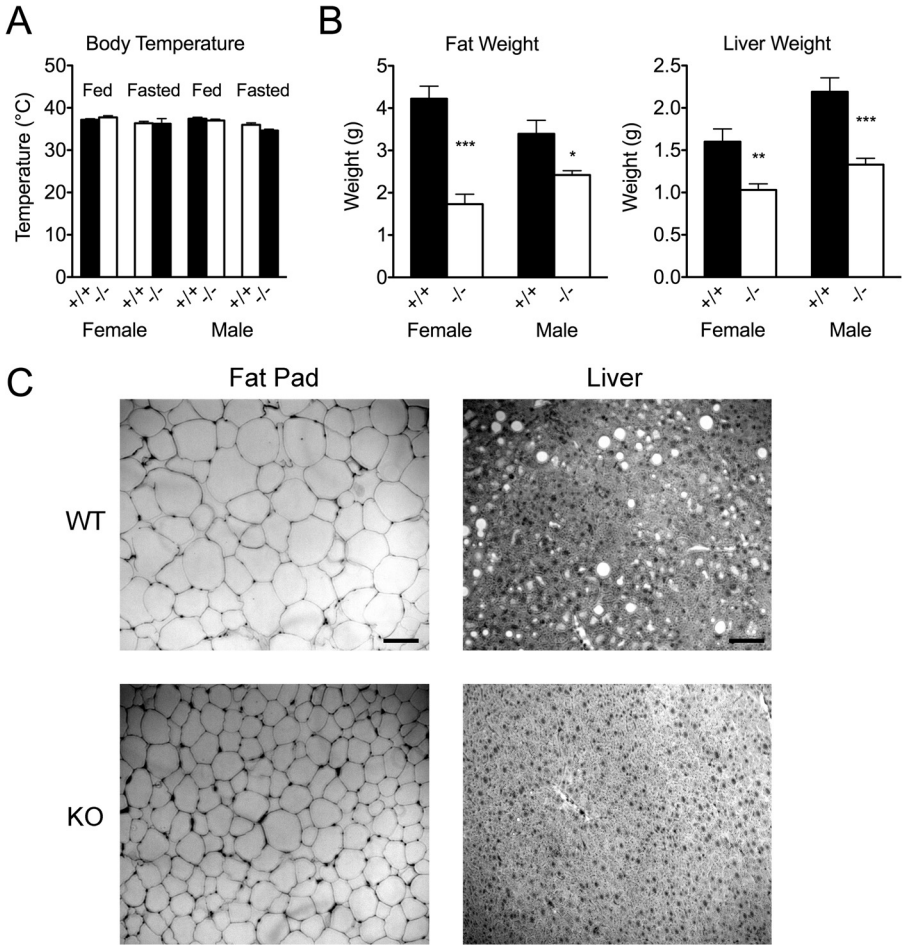

FIGURE 4. **Body temperature and tissue weight.** *A,* basal body temperature was determined rectally in free-fed or fasted adult animals ($n = 4–8$). *B,* tissues were extracted from adult (5–6 months of age) animals ($n = 5–7$), blotted dry and weighed. Fat corresponds to total abdominal cavity adipose tissue. Average values ± S.E. are plotted. Statistical significance of the differences between wild-type (+/+; WT) and *Nckx4* knock-out (−/−; KO) is indicated where present: *, $p < 0.05$; **, $p < 0.01$; ***, $p < 0.001$. *C,* microscopic images of hematoxylin and eosin-labeled sections from paraffin-embedded samples of abdominal fat pad or liver are shown. *Scale bar,* 100 μm. These images are representative of samples from at last 5 pairs of animals of each genotype.

antagonist, R_p-cAMP (Fig. 10, *E–H,* respectively). Furthermore, MSH induced a dose-dependent increase in cAMP levels in GT1–7 cells, which was not influenced by prior treatment with either U73122 or SKF96365 (Fig. 9*E*). These data support the generation of dual and mutually independent MC4R-mediated cAMP and Ca^{2+} signals, similar to dual signaling reported for the metabotropic glutamate receptor (39). The MC4R Ca^{2+} signal does not arise from intracellular release, but depends upon surface entry activated by a long-lived PLC-generated mediator, possibly diacylglycerol. Such a pathway for activation of Ca^{2+} entry has been shown for the human transient potential-like channels, TRPC3 and TRPC6 (40).

Ca^{2+}- and NCKX4-dependent Regulation of Oxytocin Expression in the PVN—To determine whether altered MC4R-induced Ca^{2+} signaling is responsible for the anorexic phenotype of the *Nckx4*$^{-/-}$ mice, we examined oxytocin (OXT) expression in PVN neurons, where it appears to play an essential MC4R-dependent role in feeding behavior, downstream from both ARGP- and POMC-neurons of the ARC (16, 41). Consistent with these data, we found that treatment of fasted wild-type mice with MSH induced a more than 2-fold increase in the number of PVN neurons expressing high levels of OXT (Fig. 11). Fasted *Nckx4*$^{-/-}$ mice contained a similar number of neurons expressing high levels of OXT as the MSH-treated wild-type, consistent with a constitutively induced level of expression. In both cases, inhibition of PLC with U73122 or surface Ca^{2+} entry channels with SKF96365, treatments that prevent MSH-induced Ca^{2+} signals but not cAMP signals, reduced the number of neurons expressing high levels of OXT to control values (Fig. 11). Thus, MSH-induced OXT expression in hypothalamic PVN neurons and the consequent suppression of food intake depend upon M4CR-generated Ca^{2+} signals. These signals are present constitutively in the *Nckx4* knock-out mice, resulting in the observed hypophagic phenotype.

DISCUSSION

In this article we have demonstrated that loss of the K^+-dependent Na^+/Ca^{2+}-exchanger protein, NCKX4, results in a specific and dramatic hypophagic response, leading to reduced fat content and lower weight in *Nckx4*$^{-/-}$ mice. We observed similar reductions in feeding and weight in two independently derived *Nckx4* knock-out lines and similar data on body weight were published recently by another group using a different gene targeting strategy (9). Our data rule out changes in circulating adiposity molecules and ARC mediators as a cause for the hypophagic behavior (see Fig. 6). The animals do not demonstrate a

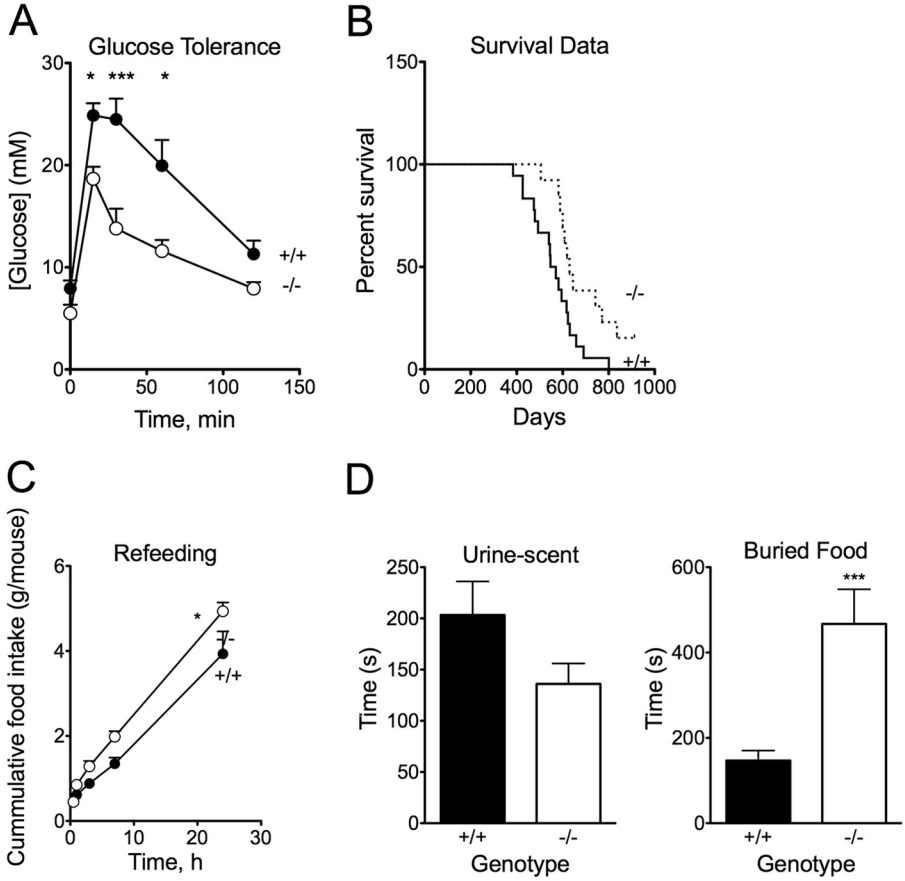

FIGURE 5. **Health parameters, motivation and olfaction in *Nckx4*$^{-/-}$ knock-out and wild-type (+/+) mice.** *A,* a glucose tolerance test was performed on 5–6-month-old animals following overnight fasting. Glucose (2 mg/g body weight) was injected intraperitoneally, and blood glucose was measured just prior and at intervals thereafter. Average values ± S.E. are plotted ($n = 6$). *B,* a Kaplan Meier survival curve is plotted for 18 wild-type (+/+) and 13 *Nckx4* knock-out (−/−) animals. A log-rank (Mantel-Cox) test indicates a significant difference between genotypes, $p < 0.05$. *C,* cumulative food consumption was measured in adult mice immediately following a 24-h fasting period ($n = 11$). *D,* time taken to find buried urine-scented litter (*left*) or buried food pellet (*right*) was measured for adult mice ($n = 11–13$). Statistical significance of the differences between genotypes determined by analysis of variance using the Bonferroni post-test is indicated where present: *, $p < 0.05$; ***, $p < 0.001$.

pervasive developmental defect, any serious health issues, nor any obvious change in morphology that might lead to the observed reduction in food intake (Figs. 2, 4, and 5). Neither do motivational factors, which can influence food intake, appear to influence the behavior of the *Nckx4* knock-out mice (Fig. 5). Thus we conclude that the loss of NCKX4 protein expression leads directly to highly specific neuronal changes underlying the reduction in food intake.

A recently published study (9) demonstrated a similar reduction of body weight in global *Nckx4* knock-out mice, an altered olfactory response, and a partial deficit in olfactory function that led to an ensuing nursing defect. Olfactory-specific *Nckx4* knock-out animals had lower body weight at weaning, although the authors did not report body weight in adult olfactory-specific knock-out animals. Our experiments on *Nckx4* knock-out animals revealed a similar deficit in olfactory performance when presented with hidden food following a fast, but not with hidden urine-scented litter (Fig. 5*D*). Although our data are consistent with a partial loss of olfactory function in *Nckx4*$^{-/-}$ mice that contributes to hypophagia, such a deficit cannot underlie the main change in feeding behavior and body weight in adult animals for the following reasons. Unlike Stephan *et al.* (9), we note a progressively increasing fractional difference in body weight from weaning age to adulthood (Fig. 3*A*). We have also directly measured a reduction in food consumption by adult *Nckx4*$^{-/-}$ mice (Fig. 3*D*). Because these animals have no difficulty finding visible food, as demonstrated in a re-feeding following the fasting experiment (Fig. 5*C*), we conclude that reduced olfactory function does not lead to reduced food consumption in an *ad libitum* feeding scenario for adult animals. Finally and most importantly, we have demonstrated an increase in both c-Fos and OXT expression in the hypothalamic PVN neurons of fasted *Nckx4*$^{-/-}$ mice that could not arise as a consequence of an olfactory deficit leading to reduced food intake (a scenario that would be expected to reduce c-Fos and OXT expression, as observed in fasted wild-type mice, see Figs. 7 and 11).

Instead, our data demonstrate that the main change in feeding behavior in the *Nckx4*$^{-/-}$ mice is caused by a constitutive activation of PVN neurons, in an MC4R-dependent and Ca^{2+}-sensitive manner, which induces an increase in OXT expression and a consequent anorexigenic response. That loss of NCKX4-driven Ca^{2+} efflux could have such a selective behavioral response is surprising. We had previously demonstrated that *Nckx4* expression is quite widely distributed among brain regions (34). This is also shown in Fig. 2*A*, where *Nckx4* tran-

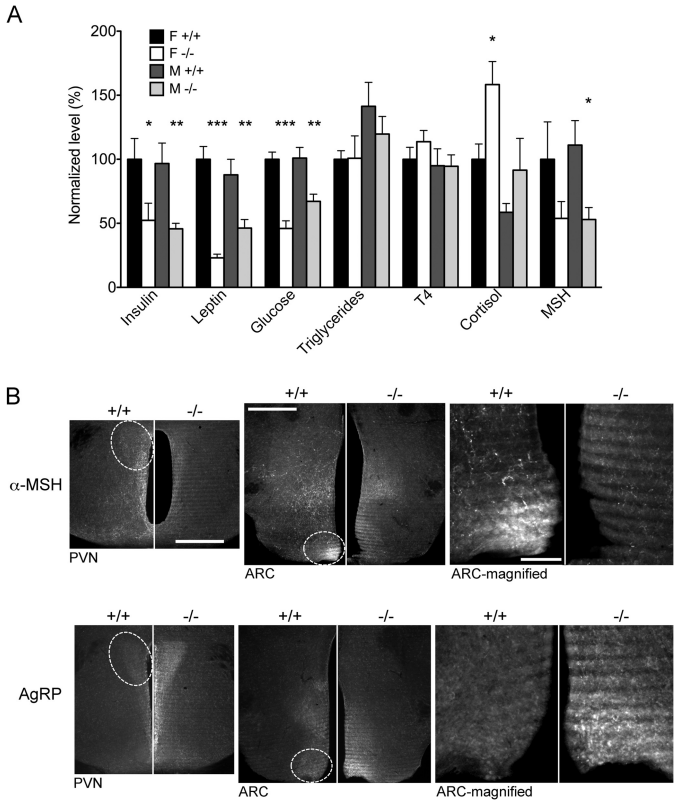

FIGURE 6. **Blood hormones and hypothalamic mediators.** *A,* serum samples from overnight fasted female (F) or male (*M*) animals of wild-type (+/+) or *Nckx4* knock-out (−/−) genotype ($n = 7–10$) were tested for the indicated factors. Levels are plotted normalized to the wild-type female levels in each case. Statistical significance of differences between knock-out and wild-type for each gender is indicated where present: *, $p < 0.05$; **, $p < 0.01$; ***, $p < 0.001$. The values corresponding to 100% are: insulin, 1.51 ng/ml; leptin, 55.5 ng/ml; glucose, 261 mg/dl; triglycerides, 0.49 mg/ml; T4, 5.0 μg/dl; cortisol, 4.1 μg/dl; MSH, 110 pmol/liter. *B,* localization of MSH and AgRP was determined by immunofluorescence in coronal sections through the hypothalamic region of adult female wild-type (+/+) or *Nckx4* knock-out (−/−) mice. For illustrative purposes, bilaterally symmetric image halves are compared between *Nckx4*$^{+/+}$ and *Nckx4*$^{-/-}$ animals for sections taken at the level of the PVN and ARC. The PVN and ARC regions are *circled*. *Scale bar*, 500 μm. The *right-hand* most image pairs are magnified views of the ARC regions from the central image pairs, illustrating the punctate nature of staining, consistent with packaging of peptide hormones in vesicles destined for secretion. *Scale bar*, 100 μm. These images are representative of three independent experiments.

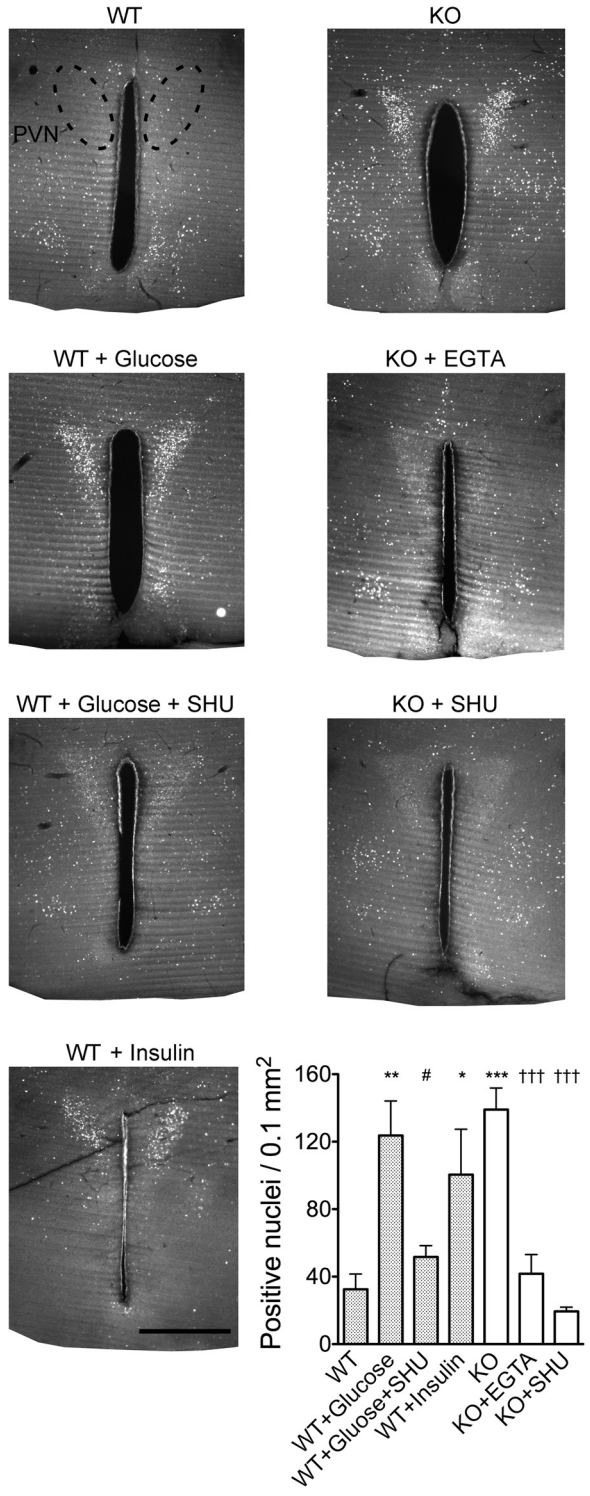

FIGURE 7. **Neurons in the PVN are activated in *Nckx4*$^{-/-}$ mice.** c-Fos expression was detected by immunofluorescence in sections from hypothalamus of adult mice. *WT*, wild-type; *KO*, *Nckx4*$^{-/-}$. All animals were fasted for 48 h and subsequently treated for 30 min prior to sacrifice either with glucose injection (intraperitoneally; 2 mg/g body weight) or by perfusion with Ca^{2+}-free Krebs-Henseleit solution containing 1 mM EGTA, normal Krebs-Henseleit solution containing 100 nM insulin, or normal Krebs-Henseleit solution containing 1 μM of the MC4R antagonist, SHU9119 (*SHU*). The total number of c-Fos positive nuclei contained within the PVN area were counted for each section, and the averaged data ± S.E. from 4 to 7 independent experiments are shown in the panel at the *lower right*. Statistical significance is indicated where present: compared with wild-type untreated: *, $p < 0.05$; **, $p < 0.01$; ***, $p < 0.001$; compared with glucose-treated wild-type: #, $p < 0.05$; compared with knock-out untreated: †††, $p < 0.001$. *Scale bar*, 500 μm.

scripts can be readily observed in the PVN. Various other Na^+/Ca^{2+}-exchangers are also broadly expressed in brain neurons, although their expression is not influenced by the loss of the NCKX4 protein (Fig. 2*C*). Moreover, no anorexic phenotype comparable with that of the *Nckx4*$^{-/-}$ mice has been observed in other Na^+/Ca^{2+}-exchanger knock-out models (30, 42–45). Furthermore, we do not observe a general defect in Ca^{2+} extrusion from neurons isolated from *Nckx4*$^{-/-}$ animals (data not shown). Thus, our results suggest that within PVN neurons NCKX4 plays a special and non-compensated role in regulating Ca^{2+} flux and signaling associated tightly with MC4R signaling linked with feeding behavior and satiety.

PVN neurons have previously been shown to play a critical role in the MSH-induced anorexic response (18, 19). This nucleus comprises a heterogenic population of neurons extending processes to other hypothalamic areas, to the pituitary, as well as to nuclei in the brain stem and spinal column (46).

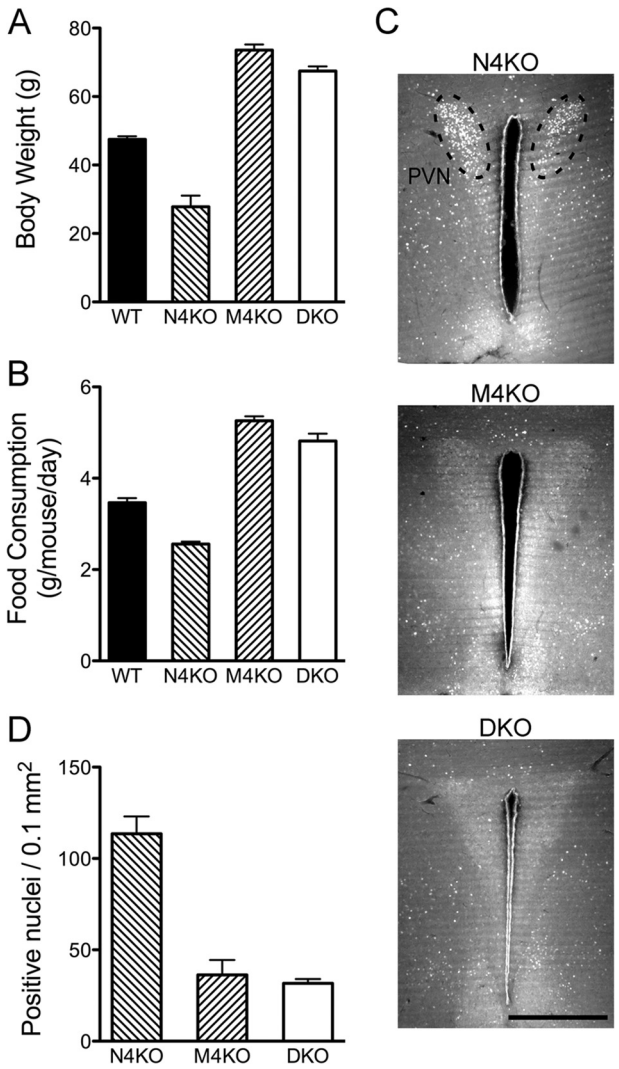

FIGURE 8. **The *Nckx4*$^{-/-}$ phenotype is MC4R-dependent**. Age-matched adult mice of different genotypes were compared: WT, wild-type; N4KO, *Nckx4*$^{-/-}$; M4KO, *Mc4r*$^{-/-}$; DKO, *Nckx4*$^{-/-}$; *Mc4r*$^{-/-}$. *A*, body weight (n = 6–9); *B*, food consumption (n = 10); *C* and *D*, c-Fos immunofluorescence in coronal hypothalamic sections of fasted animals, as described in the legend to Fig. 7 (n = 4–7). In *panels A* and *B*, N4KO, M4KO, and DKO are all significantly different from WT, and in *panels A*, *B*, and *D*, M4KO and DKO are significantly different from N4KO, with $p < 0.001$ in all cases. *Scale bar*, 500 μm.

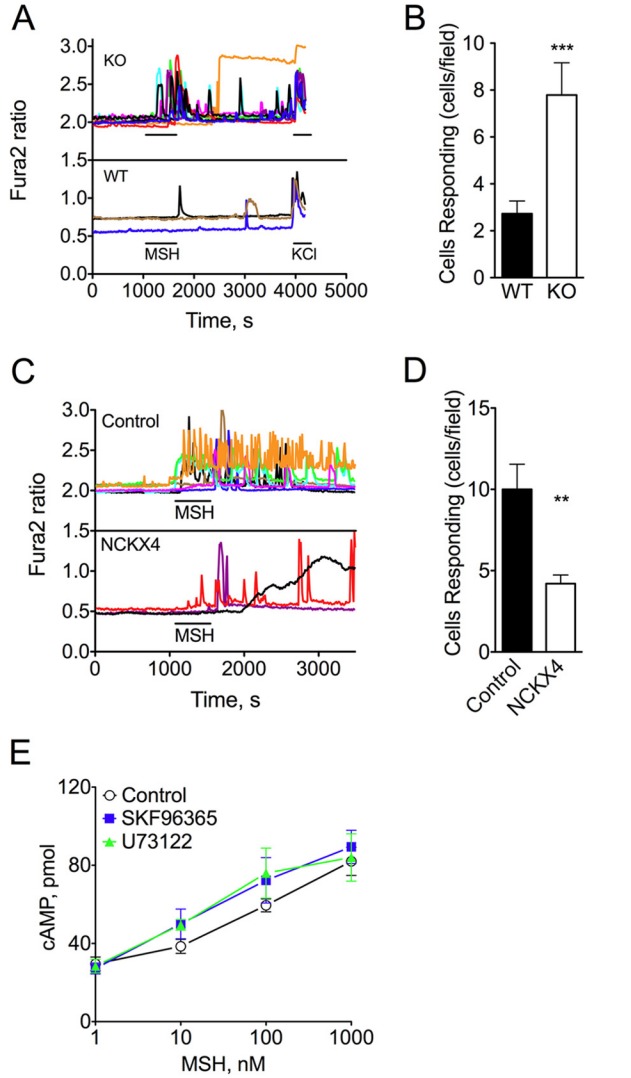

FIGURE 9. **MSH-induced Ca^{2+} signals.** *A*, the fura-2 340/380 fluorescent excitation ratios are shown for individual neurons, each plotted with a uniquely colored trace, from primary hypothalamic cultures from either wild-type (*WT*) or *Nckx4* knock-out (*KO*) mice. Cells were continually perfused with Hepes-buffered saline, containing either 1 μM MSH or 75 mM KCl where indicated. *B*, the number of cells in each microscopic field that responded with a change in fura-2 ratio, as shown in *panel A*, following MSH treatment is plotted. Averages ± S.E. for 18–20 microscopic fields from six independent cultures are shown. ***, $p < 0.001$. *C*, GT1–7 cells were infected with lentivirus expressing mouse NCKX4, or a deleted control construct, and subsequently assayed for Ca^{2+} response 2 days later. The fura-2 340/380 excitation ratios for individual responding cells are shown, each plotted with a uniquely colored trace. *D*, the average number of responding cells per field is summarized. n = 9; **, $p <$ 0.01. *E*, GT1–7 cells in Opti-MEM were treated with vehicle only (control) or with 10 μM SKF96365 or 10 μM U73122 at 37 °C for 15 min with the indicated concentration of MSH, followed by extraction and determination of cAMP levels (n = 5–8).

Although a fully integrated feeding response clearly requires multiple pathways and neuronal connections, recent studies have demonstrated an essential role for PVN OXT neurons in normal satiety-induced suppression of feeding (16, 41). Because intracerebroventricular delivery of OXT is effective in suppressing feeding, it is likely that OXT actions are mediated by pathways that connect the PVN to the brainstem and/or spinal cord, rather than those that project to the posterior pituitary (16, 41). Our data demonstrating an MSH-dependent increase in PVN OXT expression (Fig. 11) are consistent with those findings. In humans, the obesity of Prader-Willi syndrome is thought to be due to a deficiency in OXT neurons (47), and OXT administration may also be effective in the treatment of obesity (48).

The MC4R is a G-protein coupled receptor capable of signaling through $G\alpha_s$ to cAMP and protein kinase A (22). However, loss of $G\alpha_s$ expression in PVN neurons (23, 24), or selective deletion of the cAMP-response-element binding protein in PVN neurons (49), does not change feeding behavior indicating that $G\alpha_s$ signaling downstream of MC4R is not required for the satiety response. Furthermore, mutations in MC4R that are associated with changes in adipocity do not always result in consistent changes to $G\alpha_s$ signaling, suggesting that other pathways may also contribute to MC4R action (41, 50). Dual coupling has been demonstrated previously for other G-protein coupled receptors, such as the metabotropic glutamate receptor and the thyroid stimulating hormone receptor (39, 51).

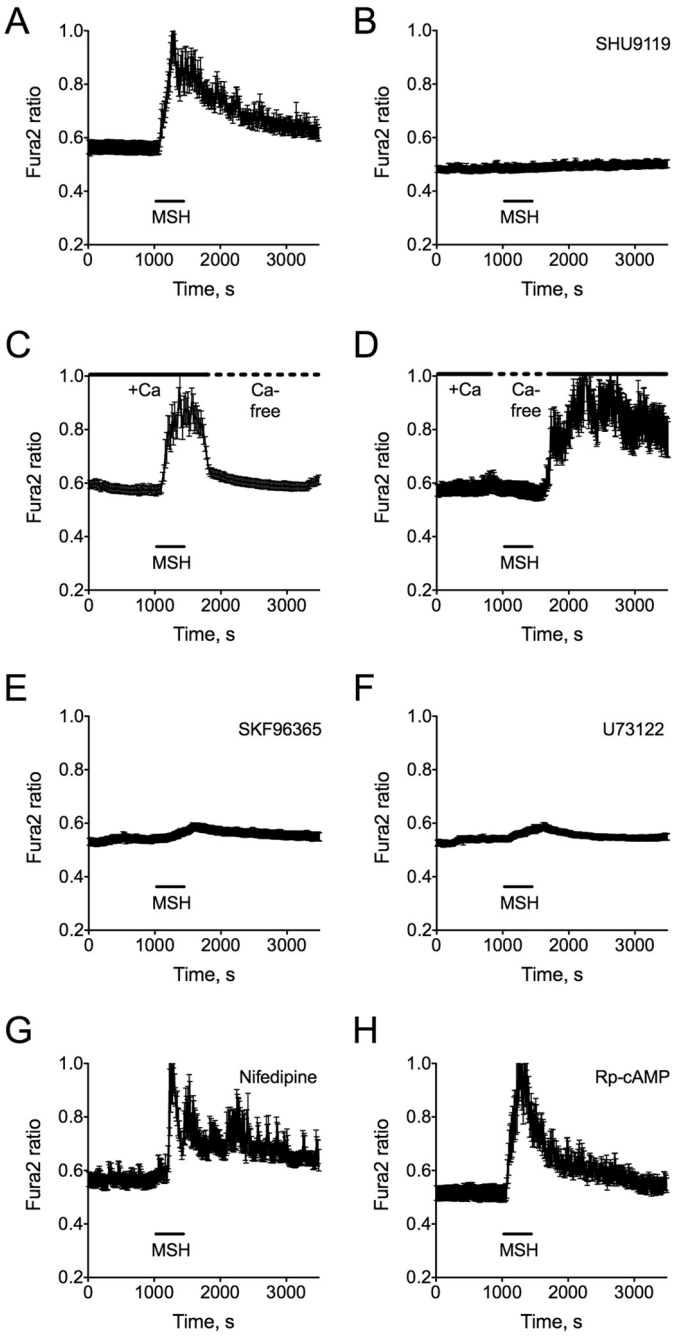

FIGURE 10. **MSH treatment induces Ca^{2+} signals in hypothalamic GT1–7 cells.** Confluent GT1–7 cells were analyzed individually for Ca^{2+} responses as described in the legend to Fig. 9. The average fura-2 ratio ± S.E. is plotted for the responding cells. *A,* the normal response of the cells to 300 s perfusion with 1 μM MSH in Hepes-buffered saline perfusate containing 2 mM $CaCl_2$ (n = 17). *B,* cells were pretreated with 1 μM SHU9119 for 15 min prior to application of MSH (n = 14). *C,* following activation by MSH treatment in normal perfusate (*+Ca*), 200 s later the perfusate was switched one without $CaCl_2$ containing 0.1 mM EGTA (*Ca-free*) (n = 15). *D,* cells were switched from normal perfusate (*+Ca*) to one without $CaCl_2$ containing 0.1 mM EGTA for 500 s (Ca-free) during which MSH was applied for 300 s (n = 9). *E,* cells were pretreated with 10 μM SKF96365 for 15 min prior to application of MSH (n = 11). *F,* cells were pretreated with 10 μM U73122 for 15 min prior to application of MSH (n = 11). *G,* cells were pretreated with 50 μM nifedipine for 15 min prior to application of MSH (n = 9). *H,* cells were pretreated with 100 μM R_p-cAMP for 15 min prior to application of MSH (n = 17). These data are representative of at least six different coverslips from three different experiments for each condition. Anywhere from 7 to 25 cells per microscopic field, with an average of 15 cells, responded to MSH stimulation in each experiment. The number of responding cells was not different for cells pretreated with nifedipine or R_p-cAMP.

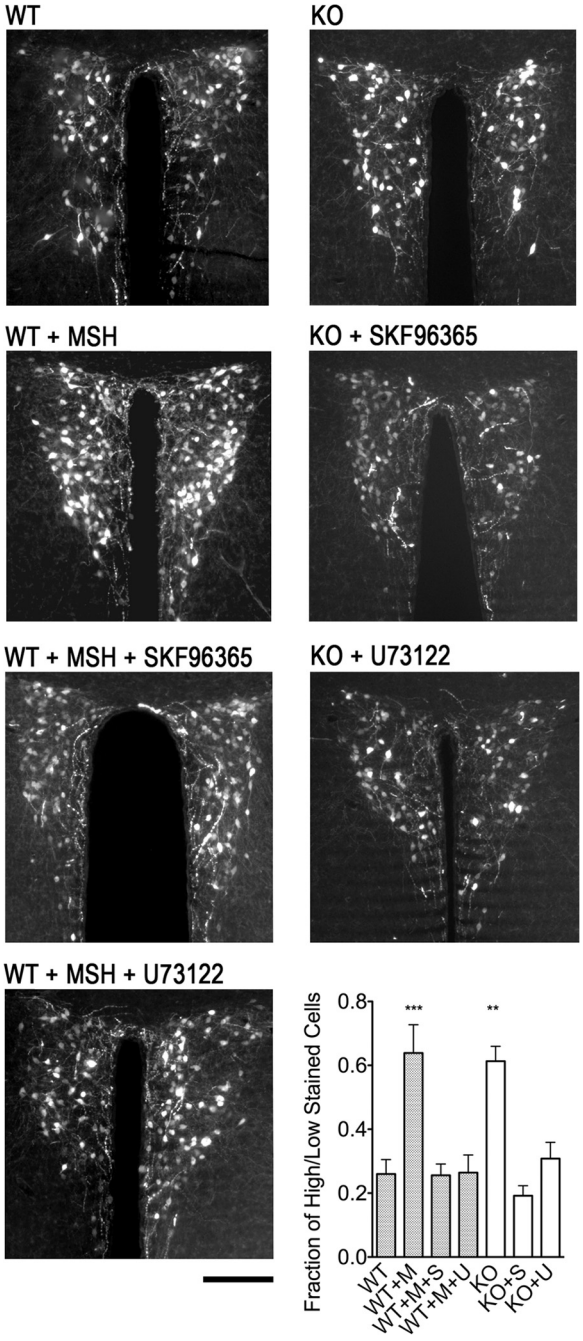

FIGURE 11. **Control of oxytocin expression in the hypothalamic paraventricular nucleus.** Oxytocin expression was detected by immunofluorescence in adult mice. *WT*, wild-type; *KO*, *Nckx4*$^{-/-}$. Animals were fasted for 48 h and then subjected to a 30-min transcardial perfusion with Krebs-Henseleit solution containing 1 μM MSH, 10 μM SKF96365, or 10 μM U73122, as indicated. The oxytocin-positive cells were scored as being of high or low staining intensity, and the numbers pooled across all sections from each of five animals per treatment group. The total number of cells scored varied from 522 to 1288 per animal, but the averaged values were not different between groups (800 cells). The averaged ratios of high/low stained cells ± S.E. are shown in the panel at *lower right*. Statistical significance is indicated where present: compared with wild-type untreated: **, $p < 0.01$; ***, $p < 0.001$. *Scale bar*, 100 μm.

Although there have been previous reports showing Ca^{2+} signals in response to MSH treatment of cultured cells (52, 53), to our knowledge no previous report has demonstrated an essential role for MC4R-mediated Ca^{2+} signals in suppression of feeding. Our hypothesis for the mechanism linking MC4R

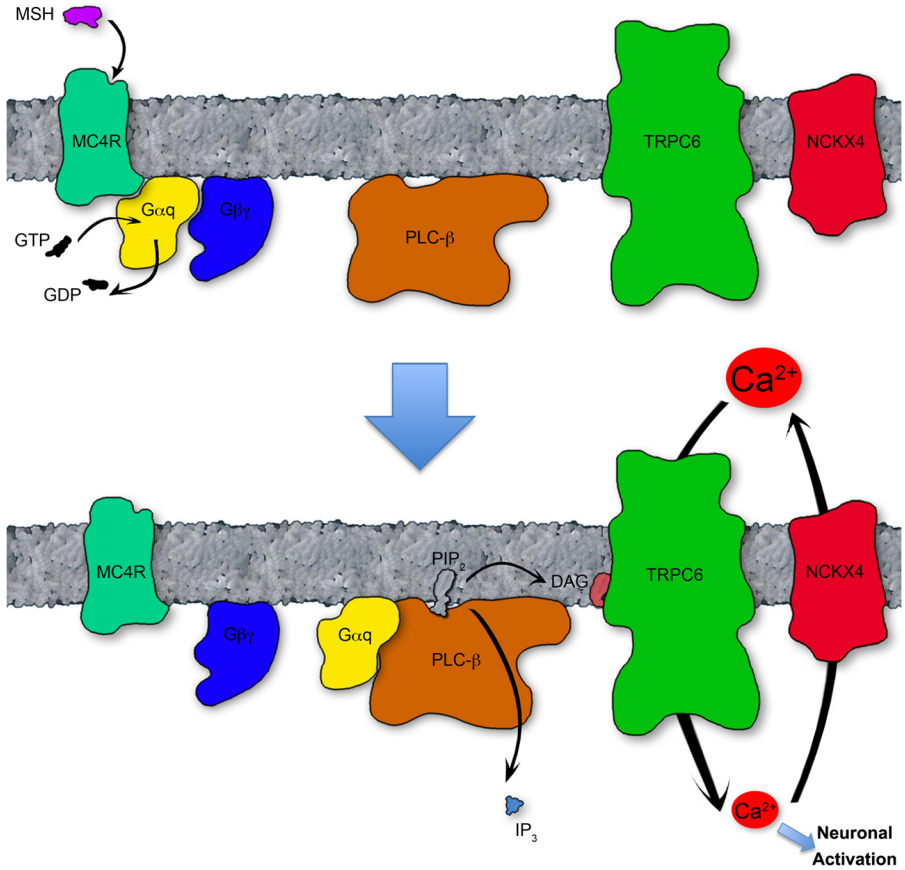

FIGURE 12. **A model for MC4R-dependent Ca^{2+} signaling and the role of NCKX4.** MSH binding to the MC4R is shown to active $G\alpha_q$, via the exchange of GTP for GDP (*upper row*). It is important to note that MC4R may constitutively activate $G\alpha_q$ even in the absence of ligand (54). So activated, $G\alpha_q$ goes on to bind and stimulate PLC-β, which subsequently cleaves phosphatidylinositol 1,4-bisphosphate (*PIP_2*) to diacylglycerol (*DAG*) and inositol 1,4,5-trisphosphate (*IP_3*). The membrane-bound diacylglycerol then activates the Ca^{2+}-selective entry channel, TRPC6, which results in an elevation of cytosolic [Ca^{2+}] and consequent neuronal activation, which may include the initiation of action potentials (15) and the release of oxytocin (16, 41) (*lower row*). Normally, NCKX4 acts locally to extrude the Ca^{2+} that enters via TRPC6, thus moderating the signaling pathway so only strong signals drive neuronal activation. In the absence of this moderating influence, even weak, constitutive, signaling via MC4R can result in sufficient Ca^{2+} entry to initiate neuronal activation.

stimulation with neuronal activation that leads to satiety signaling, and the role for NCKX4 activity in this process, is illustrated in the schematic of Fig. 12. The central findings from this study that support our model are as follows. First, we demonstrate that MSH treatment induces prominent oscillatory and long-lived Ca^{2+} signals that are sensitive to the MC4R antagonist, SHU9119 (see Fig. 10). These Ca^{2+} signals are blocked by the PLC inhibitor, U73122, or by the TRPC-selective Ca^{2+} entry inhibitor, SKF96365, but not the voltage-dependent Ca^{2+} channel inhibitor, nifedipine, suggesting that MC4R can couple through $G\alpha_q$ to the activation of PLC, the production of diacylglycerol, and the activation of surface Ca^{2+} entry channels, such as TRPC3 or TRPC6 (40). Second, MSH also induces an increase in cAMP, a response that is not influenced by treatment with either U73122 or SKF96365 (Fig. 9*E*), suggesting that MC4R can signal independently via both $G\alpha_s$ and $G\alpha_q$, as also demonstrated for other G-protein coupled receptors (39, 51). Third, the MSH induced production of OXT in PVN can be prevented by U73122 or SKF96365 (Fig. 11), thus implicating Ca^{2+}, but not cAMP, signals in the normal suppression of feeding during satiety. In support of this essential role for Ca^{2+} signaling, the *Nckx4* knock-out mice have a constitutive activation of OXT expression, which can also be blocked by U73122 or SKF96365 (Fig. 11).

Our data clearly demonstrate that loss of the Ca^{2+} transporter, NCKX4, in the *Nckx4*$^{-/-}$ mice leads to a specific change in the melanocortin signaling axis that results in the constitutive activation of PVN neurons and the induction of anorexia. In our studies this is evidenced by an elevation of c-Fos expression and OXT expression in PVN neurons, and by a change in the number of neurons that respond with Ca^{2+} signals to MSH stimulation. Because K^+-dependent Na^+/Ca^{2+}-exchangers like NCKX4 are thermodynamically poised to catalyze Ca^{2+} extrusion, loss of this pathway in *Nckx4*$^{-/-}$ animals may destabilize normal Ca^{2+} homeostasis, so that normally subthreshold signals through the MC4R trigger a sustained response. This may be particularly important for MC4R function, because the receptor is known to possess constitutive activity even in the absence of ligand (54), and because once a Ca^{2+} response has been initiated, it remains long lived (see Figs. 9 and 10). Previous studies have demonstrated that NCKX exchangers typically play a significant role in Ca^{2+} homeostasis in environments where Ca^{2+} flux is high and intracellular Ca^{2+} levels rise substantially, in a temporally and/or spatially restricted manner (3, 55). This suggests that NCKX4 may be localized in close proximity to the entry pathways that control Ca^{2+} signaling downstream from the MC4R (see model in Fig. 12). Such a specialized location may also explain why NCKX4 has a non-compensated

and selective role in Ca^{2+} homeostasis associated with the hypothalamic melanocortin axis. Selective roles for NCKX4 in other cells and tissues may also depend upon the precise subcellular distribution of the NCKX4 protein in relationship to components of other signaling pathways. These concepts await further investigation.

Acknowledgments—We thank Dr. Jaideep Bains (University of Calgary) for providing critical comments and essential suggestions, Dr. Richard Weiner (University of California at San Francisco) for GT1–7 cells, Dr. Frank Visser (University of Calgary) for lentiviral packaging and amplification, Guang Yang (University of Calgary) for technical assistance in mouse genotyping, and Elena Miklyaeva (University of Calgary) for mouse behavior screening.

REFERENCES

1. Berridge, M. J. (1998) Neuronal calcium signaling. *Neuron* **21,** 13–26
2. Berridge, M. J., Bootman, M. D., and Roderick, H. L. (2003) Calcium signalling: dynamics, homeostasis and remodelling. *Nat. Rev. Mol. Cell Biol.* **4,** 517–529
3. Lee, S. H., Kim, M. H., Park, K. H., Earm, Y. E., and Ho, W. K. (2002) K^+-dependent Na^+/Ca^{2+} exchange is a major Ca^{2+} clearance mechanism in axon terminals of rat neurohypophysis. *J. Neurosci.* **22,** 6891–6899
4. Kim, M. H., Lee, S. H., Park, K. H., and Ho, W. K. (2003) Distribution of K^+-dependent Na^+/Ca^{2+} exchangers in the rat supraoptic magnocellular neuron is polarized to axon terminals. *J. Neurosci.* **23,** 11673–11680
5. Lytton, J. (2007) Na^+/Ca^{2+} exchangers: three mammalian gene families control Ca^{2+} transport. *Biochem. J.* **406,** 365–382
6. Visser, F., and Lytton, J. (2007) K^+-dependent Na^+/Ca^{2+} exchangers: key contributors to Ca^{2+} signaling. *Physiology* **22,** 185–192
7. Schnetkamp, P. P. (2004) The SLC24 Na^+/Ca^{2+}-K^+ exchanger family: vision and beyond. *Pflugers Arch.* **447,** 683–688
8. Lamason, R. L., Mohideen, M. A., Mest, J. R., Wong, A. C., Norton, H. L., Aros, M. C., Jurynec, M. J., Mao, X., Humphreville, V. R., Humbert, J. E., Sinha, S., Moore, J. L., Jagadeeswaran, P., Zhao, W., Ning, G., Makalowska, I., McKeigue, P. M., O'donnell, D., Kittles, R., Parra, E. J., Mangini, N. J., Grunwald, D. J., Shriver, M. D., Canfield, V. A., and Cheng, K. C. (2005) SLC24A5, a putative cation exchanger, affects pigmentation in zebrafish and humans. *Science* **310,** 1782–1786
9. Stephan, A. B., Tobochnik, S., Dibattista, M., Wall, C. M., Reisert, J., and Zhao, H. (2012) The Na^+/Ca^{2+} exchanger NCKX4 governs termination and adaptation of the mammalian olfactory response. *Nat. Neurosci.* **15,** 131–137
10. Parry, D. A., Poulter, J. A., Logan, C. V., Brookes, S. J., Jafri, H., Ferguson, C. H., Anwari, B. M., Rashid, Y., Zhao, H., Johnson, C. A., Inglehearn, C. F., and Mighell, A. J. (2013) Identification of mutations in SLC24A4, encoding a potassium-dependent sodium/calcium exchanger, as a cause of amelogenesis imperfecta. *Am. J. Hum. Genet.* **92,** 307–312
11. Cone, R. D. (2005) Anatomy and regulation of the central melanocortin system. *Nat. Neurosci.* **8,** 571–578
12. Gao, Q., and Horvath, T. L. (2007) Neurobiology of feeding and energy expenditure. *Annu. Rev. Neurosci.* **30,** 367–398
13. Morton, G. J., Cummings, D. E., Baskin, D. G., Barsh, G. S., and Schwartz, M. W. (2006) Central nervous system control of food intake and body weight. *Nature* **443,** 289–295
14. Aponte, Y., Atasoy, D., and Sternson, S. M. (2011) AGRP neurons are sufficient to orchestrate feeding behavior rapidly and without training. *Nat. Neurosci.* **14,** 351–355
15. Ghamari-Langroudi, M., Srisai, D., and Cone, R. D. (2011) Multinodal regulation of the arcuate/paraventricular nucleus circuit by leptin. *Proc. Natl. Acad. Sci. U.S.A.* **108,** 355–360
16. Atasoy, D., Betley, J. N., Su, H. H., and Sternson, S. M. (2012) Deconstruction of a neural circuit for hunger. *Nature* **488,** 172–177
17. Huszar, D., Lynch, C. A., Fairchild-Huntress, V., Dunmore, J. H., Fang, Q., Berkemeier, L. R., Gu, W., Kesterson, R. A., Boston, B. A., Cone, R. D., Smith, F. J., Campfield, L. A., Burn, P., and Lee, F. (1997) Targeted disruption of the melanocortin-4 receptor results in obesity in mice. *Cell* **88,** 131–141
18. Cowley, M. A., Pronchuk, N., Fan, W., Dinulescu, D. M., Colmers, W. F., and Cone, R. D. (1999) Integration of NPY, AGRP, and melanocortin signals in the hypothalamic paraventricular nucleus: evidence of a cellular basis for the adipostat. *Neuron* **24,** 155–163
19. Balthasar, N., Dalgaard, L. T., Lee, C. E., Yu, J., Funahashi, H., Williams, T., Ferreira, M., Tang, V., McGovern, R. A., Kenny, C. D., Christiansen, L. M., Edelstein, E., Choi, B., Boss, O., Aschkenasi, C., Zhang, C. Y., Mountjoy, K., Kishi, T., Elmquist, J. K., and Lowell, B. B. (2005) Divergence of melanocortin pathways in the control of food intake and energy expenditure. *Cell* **123,** 493–505
20. Farooqi, I. S., and O'Rahilly, S. (2008) Mutations in ligands and receptors of the leptin-melanocortin pathway that lead to obesity. *Nat. Clin. Pract. Endocrinol. Metab.* **4,** 569–577
21. Loos, R. J. (2011) The genetic epidemiology of melanocortin 4 receptor variants. *Eur. J. Pharmacol.* **660,** 156–164
22. Adan, R. A., Tiesjema, B., Hillebrand, J. J., la Fleur, S. E., Kas, M. J., and de Krom, M. (2006) The MC4 receptor and control of appetite. *Br. J. Pharmacol.* **149,** 815–827
23. Chen, M., Wang, J., Dickerson, K. E., Kelleher, J., Xie, T., Gupta, D., Lai, E. W., Pacak, K., Gavrilova, O., and Weinstein, L. S. (2009) Central nervous system imprinting of the G protein $G\alpha_s$ and its role in metabolic regulation. *Cell Metab.* **9,** 548–555
24. Chen, M., Berger, A., Kablan, A., Zhang, J., Gavrilova, O., and Weinstein, L. S. (2012) $G\alpha_s$ deficiency in the paraventricular nucleus of the hypothalamus partially contributes to obesity associated with $G\alpha_s$ mutations. *Endocrinology* **153,** 4256–4265
25. Tsuzuki, T., and Rancourt, D. E. (1998) Embryonic stem cell gene targeting using bacteriophage λ vectors generated by phage-plasmid recombination. *Nucleic Acids Res.* **26,** 988–993
26. Marth, J. D. (1996) Recent advances in gene mutagenesis by site-directed recombination. *J. Clin. Invest.* **97,** 1999–2002
27. Yang, X., and Lytton, J. (2013) Purinergic stimulation of K^+-dependent Na^+/Ca^{2+} exchanger isoform 4 requires dual activation by PKC and CaMKII. *Biosci. Rep.* **33,** e00087
28. Gunaydin, L. A., Yizhar, O., Berndt, A., Sohal, V. S., Deisseroth, K., and Hegemann, P. (2010) Ultrafast optogenetic control. *Nat. Neurosci.* **13,** 387–392
29. Ausubel, F. M., Brent, R., Kingston, R. E., Moore, D. D., Seidman, J. G., Smith, J. A., and Struhl, K. (eds) (2012) *Current Protocols in Molecular Biology*, John Wiley & Sons, New York
30. Li, X. F., Kiedrowski, L., Tremblay, F., Fernandez, F. R., Perizzolo, M., Winkfein, R. J., Turner, R. W., Bains, J. S., Rancourt, D. E., and Lytton, J. (2006) Importance of K^+-dependent Na^+/Ca^{2+}-exchanger 2, NCKX2, in motor learning and memory. *J. Biol. Chem.* **281,** 6273–6282
31. Crawley, J. N. (1999) Behavioral phenotyping of transgenic and knockout mice: experimental design and evaluation of general health, sensory functions, motor abilities, and specific behavioral tests. *Brain Res.* **835,** 18–26
32. Yang, M., and Crawley, J. N. (2009) Simple behavioral assessment of mouse olfaction. *Curr. Protoc. Neurosci.*, Chapter 8, Unit 8.24, 10.1002/0471142301.ns0824s48
33. Mellon, P. L., Windle, J. J., Goldsmith, P. C., Padula, C. A., Roberts, J. L., and Weiner, R. I. (1990) Immortalization of hypothalamic GnRH neurons by genetically targeted tumorigenesis. *Neuron* **5,** 1–10
34. Li, X. F., Kraev, A. S., and Lytton, J. (2002) Molecular cloning of a fourth member of the potassium-dependent sodium-calcium exchanger gene family, NCKX4. *J. Biol. Chem.* **277,** 48410–48417
35. Fontana, L., Partridge, L., and Longo, V. D. (2010) Extending healthy life span: from yeast to humans. *Science* **328,** 321–326
36. Shimada, M., Tritos, N. A., Lowell, B. B., Flier, J. S., and Maratos-Flier, E. (1998) Mice lacking melanin-concentrating hormone are hypophagic and lean. *Nature* **396,** 670–674
37. Singru, P. S., Sánchez, E., Fekete, C., and Lechan, R. M. (2007) Importance of melanocortin signaling in refeeding-induced neuronal activation and satiety. *Endocrinology* **148,** 638–646
38. Khong, K., Kurtz, S. E., Sykes, R. L., and Cone, R. D. (2001) Expression of

functional melanocortin-4 receptor in the hypothalamic GT1–1 cell line. *Neuroendocrinology* **74,** 193–201
39. Tateyama, M., and Kubo, Y. (2006) Dual signaling is differentially activated by different active states of the metabotropic glutamate receptor 1α. *Proc. Natl. Acad. Sci. U.S.A.* **103,** 1124–1128
40. Hofmann, T., Obukhov, A. G., Schaefer, M., Harteneck, C., Gudermann, T., and Schultz, G. (1999) Direct activation of human TRPC6 and TRPC3 channels by diacylglycerol. *Nature* **397,** 259–263
41. Sabatier, N., Leng, G., and Menzies, J. (2013) Oxytocin, feeding, and satiety. *Front. Endocrinol. (Lausanne)* **4,** 35
42. Jeon, D., Yang, Y. M., Jeong, M. J., Philipson, K. D., Rhim, H., and Shin, H. S. (2003) Enhanced learning and memory in mice lacking Na^+/Ca^{2+} exchanger 2. *Neuron* **38,** 965–976
43. Molinaro, P., Viggiano, D., Nisticò, R., Sirabella, R., Secondo, A., Boscia, F., Pannaccione, A., Scorziello, A., Mehdawy, B., Sokolow, S., Herchuelz, A., Di Renzo, G. F., and Annunziato, L. (2011) Na^+-Ca^{2+} exchanger (NCX3) knock-out mice display an impairment in hippocampal long-term potentiation and spatial learning and memory. *J. Neurosci.* **31,** 7312–7321
44. Sokolow, S., Manto, M., Gailly, P., Molgó, J., Vandebrouck, C., Vanderwinden, J. M., Herchuelz, A., and Schurmans, S. (2004) Impaired neuromuscular transmission and skeletal muscle fiber necrosis in mice lacking Na/Ca exchanger 3. *J. Clin. Invest.* **113,** 265–273
45. Vogel, P., Read, R. W., Vance, R. B., Platt, K. A., Troughton, K., and Rice, D. S. (2008) Ocular albinism and hypopigmentation defects in $Slc24a5^{-/-}$ mice. *Vet. Pathol.* **45,** 264–279
46. Biag, J., Huang, Y., Gou, L., Hintiryan, H., Askarinam, A., Hahn, J. D., Toga, A. W., and Dong, H. W. (2012) Cyto- and chemoarchitecture of the hypothalamic paraventricular nucleus in the C57BL/6J male mouse: a study of immunostaining and multiple fluorescent tract tracing. *J. Comp. Neurol.* **520,** 6–33
47. Swaab, D. F., Purba, J. S., and Hofman, M. A. (1995) Alterations in the hypothalamic paraventricular nucleus and its oxytocin neurons (putative satiety cells) in Prader-Willi syndrome: a study of five cases. *J. Clin. Endocrinol. Metab.* **80,** 573–579
48. Zhang, H., Wu, C., Chen, Q., Chen, X., Xu, Z., Wu, J., and Cai, D. (2013) Treatment of obesity and diabetes using oxytocin or analogs in patients and mouse models. *PloS One* **8,** e61477
49. Chiappini, F., Cunha, L. L., Harris, J. C., and Hollenberg, A. N. (2011) Lack of cAMP-response element-binding protein 1 in the hypothalamus causes obesity. *J. Biol. Chem.* **286,** 8094–8105
50. Breit, A., Büch, T. R., Boekhoff, I., Solinski, H. J., Damm, E., and Gudermann, T. (2011) Alternative G protein coupling and biased agonism: new insights into melanocortin-4 receptor signalling. *Mol. Cell. Endocrinol.* **331,** 232–240
51. Neumann, S., Krause, G., Claus, M., and Paschke, R. (2005) Structural determinants for G protein activation and selectivity in the second intracellular loop of the thyrotropin receptor. *Endocrinology* **146,** 477–485
52. Mountjoy, K. G., Kong, P. L., Taylor, J. A., Willard, D. H., and Wilkison, W. O. (2001) Melanocortin receptor-mediated mobilization of intracellular free calcium in HEK293 cells. *Physiol. Genomics* **5,** 11–19
53. Newman, E. A., Chai, B. X., Zhang, W., Li, J. Y., Ammori, J. B., and Mulholland, M. W. (2006) Activation of the melanocortin-4 receptor mobilizes intracellular free calcium in immortalized hypothalamic neurons. *J. Surg. Res.* **132,** 201–207
54. Srinivasan, S., Lubrano-Berthelier, C., Govaerts, C., Picard, F., Santiago, P., Conklin, B. R., and Vaisse, C. (2004) Constitutive activity of the melanocortin-4 receptor is maintained by its N-terminal domain and plays a role in energy homeostasis in humans. *J. Clin. Invest.* **114,** 1158–1164
55. Kim, M. H., Korogod, N., Schneggenburger, R., Ho, W. K., and Lee, S. H. (2005) Interplay between Na^+/Ca^{2+} exchangers and mitochondria in Ca^{2+} clearance at the calyx of Held. *J. Neurosci.* **25,** 6057–6065